COVER SHEET

Title: On the Effect of Electrical Impedance Tomography Error and Regularization Norms for Damage Identification in Piezoresistive Composites

Authors: Tyler Tallman

ABSTRACT

Electrical impedance tomography (EIT) is a promising tool for the structural health monitoring (SHM) of composites that have been modified to be piezoresistive by the addition of carbon-based nanofillers. However, most studies have formulated the EIT problem to minimize an error vector in the least-squares sense while simultaneously using a least-squares term for regularization. This approach has important limitations in the context of SHM such as being extremely sensitive to outlier data due to damaged or faulty electrodes. Utilizing a least-squares term for regularization also makes EIT unable to image discontinuous conductivity losses such as those induced by fracture events. More sophisticated techniques that surmount these limitations have been studied in medical and mathematical venues, but these methods have not been thoroughly explored for piezoresistive imaging in SHM. Therefore, this article explores the effect of different error minimization and regularization norms on the ability of EIT to image impact damage in a carbon black (CB)-modified glass fiber/epoxy laminate.

INTRODUCTION

Structural health monitoring (SHM) has great potential in aerospace applications [1] where the consequences of a catastrophic failure can be significant. A promising approach to SHM is through the use of self-sensing materials wherein some intrinsic property of the structure itself is monitored to identify damage. To this end, piezoresistive nanocomposites have shown considerable potential [2]. In this approach, nanofillers such as carbon nanotubes (CNTs), carbon nanofibers (CNFs), or carbon black (CB) are dispersed throughout a polymeric matrix. With sufficiently many nanofillers, the material becomes electrically conductive. Furthermore, the electrical conductivity of nanofiller-modified polymers intrinsically depends on mechanical effects such as strain and damage. This means that strain or damage can be identified by monitoring changes of electrical conductivity in the material.

Beyond just detecting the occurrence of damage, it is desirable to spatially locate and image damage. For this, electrical impedance tomography (EIT) has been utilized for piezoresistive visualization in numerous material systems such as cementitious materials [3] [4] [5] [6] [7], nanocomposite thin films [8] [9] [10] [11], carbon fiber reinforced composites [12], and nanofiller-modified composites [13] [14] [15] [16] [17] [18] [19]. Interest in EIT for conductivity-based SHM is based on several features. First, EIT is low cost. Second, EIT is capable of rendering images in nearly real time. And third, there is no possibility of EIT exacerbating existing damage through mechanical interrogation. Nonetheless, EIT does have some important limitations. For example, the prevailing EIT formulation is extremely sensitive to outlier data and is incapable of resolving discontinuous, fracture-induced conductivity losses. To appreciate the source of these limitations, it is necessary to have some understanding of the EIT formulation. EIT is typically formulated as a regularized minimization problem in which the minimization and the regularization terms both take on a least-squares form. Consistent with least-squares minimization, outlier measurements substantially affect the results. Furthermore, utilizing a square term for regularization promotes spatially smooth conductivity distributions. This is at odds with discrete damage events that result in discontinuous conductivity changes. Despite these limitations, this particular EIT formulation has been most commonly used in the SHM and NDE communities because it is the most readily implemented.

Although these issues have been relatively unexplored in SHM venues, they have been dutifully treated by the medical and mathematical EIT communities [20] [21] [22]. In these studies, different minimization and regularization schemes have been explored to increase the robustness of EIT in the presence of outlier data and to produce images with discontinuous conductivity changes. Therefore, the objective of this article is to investigate the effect of different error minimization and regularization norms on the ability of EIT to image impact damage-induced conductivity changes in a CB-modified glass fiber/epoxy laminate.

The remainder of this investigation is organized as follows. First, the general formulation of EIT will be presented. Next, four approaches with different minimization and regularization combinations will be outlined. These different formulations are then used to produce images from previously published data on low velocity impact damage in a glass fiber/epoxy laminate with CB filler [17]. This will elucidate the effect of different EIT formulations on damage identification in a fiber-reinforced composite. Next, the imaging process is repeated with the inclusion of a strong, artificially-induced outlier measurement in order to study the robustness of each formulation in the presence of a faulty or damaged electrodes. Lastly, a brief summary and conclusion is presented.

ELECTRICAL IMPEDANCE TOMOGRAPHY

EIT images the internal conductivity distribution of a domain. The domain to be imaged is lined with electrodes along its periphery, and current is injected between electrode pairs while the resulting voltage is measured between electrode pairs not actively involved in the current injection. EIT seeks to determine the conductivity distribution that gives rise to the observed boundary voltages for the prescribed

current injections. This can be formulated as a minimization problem that minimizes the difference between a vector of experimentally measured voltages, $\boldsymbol{V}$, and another vector of numerically predicted voltages, $\boldsymbol{F}(\sigma)$. The process of numerically predicting the voltages is referred to as the forward problem and is typically performed using the finite element method [23]. The minimization between the measured and predicted voltages is achieved by iteratively updating the conductivity distribution, σ, supplied to the forward operator until the norm of $\boldsymbol{V} - \boldsymbol{F}(\sigma)$ is acceptably low.

Rather than recovering the absolute conductivity distribution, it is standard to utilize time difference data. This means that voltage measurements are collected from the domain to be imaged at one time and again at some later time, t_1 and t_2 respectively. It is assumed that some event (e.g. damage) has occurred between the measurements that results in a conductivity change in the domain. In this light, define the vector $\boldsymbol{y}$ as the difference between experimentally measured voltages at times t_1 and t_2 as shown below in equation (1).

$$\boldsymbol{y} = \boldsymbol{V}(t_2) - \boldsymbol{V}(t_1) \tag{1}$$

An analogous voltage difference vector can be formed from the numerical simulation as $\boldsymbol{F}(\boldsymbol{\sigma} + \boldsymbol{x}) - \boldsymbol{F}(\boldsymbol{\sigma})$. Note that the conductivity distribution, $\boldsymbol{\sigma}$, has been boldfaced to indicate that it has been discretized via the finite element method. Furthermore, the conductivity difference between times t_1 and t_2 is expressed as $\boldsymbol{x}$. Next, linearize $\boldsymbol{F}(\boldsymbol{\sigma} + \boldsymbol{x})$ by performing a Taylor series expansion as $\boldsymbol{F}(\boldsymbol{\sigma} + \boldsymbol{x}) \approx \boldsymbol{F}(\boldsymbol{\sigma}_0) + \boldsymbol{J}\boldsymbol{x}$. In the preceding, $\boldsymbol{J}$ is the sensitivity matrix and formed as $\boldsymbol{J} = \partial \boldsymbol{F}(\boldsymbol{\sigma}_0)/\partial \boldsymbol{\sigma}$ where $\boldsymbol{\sigma}_0$ is an initial estimate of the conductivity distribution. With this in mind, the regularized EIT minimization can be formally stated as follows.

$$\arg\min_{\boldsymbol{x}} \|\boldsymbol{J}\boldsymbol{x} - \boldsymbol{y}\|_m^m + \lambda \|\boldsymbol{R}\boldsymbol{x}\|_n^n \tag{2}$$

In equation (2), $\boldsymbol{R}$ represents a generic regularization term the contribution of which is controlled by the scalar λ. Furthermore, the subscript m and n terms represent the norms of the error minimization and regularization terms. The superscript m and n terms represent the power to which the norm is taken. In the following, different minimization and regularization combinations using $m = 2$ and $n = 2$, $m = 2$ and $n = 1$, $m = 1$ and $n = 2$, and $m = 1$ and $n = 1$ will be investigated. Each combination of error minimization and regularization norms has different advantages and limitations making them more or less well-suited for strain or damage imaging and more or less robust to outlier data due to damaged electrodes.

L2 ERROR NORM AND L2 REGULARIZATION NORM

First, consider equation (2) with $m = n = 2$. Both the error minimization and regularization take the form of a least-squares problem as shown in equation (3). Because the forward operator has been linearized, this minimization can be solved in one step. The explicit solution to the conductivity change is shown in equation (4).

$$\arg\min_{\boldsymbol{x}} \frac{1}{2}\|\boldsymbol{J}\boldsymbol{x}-\boldsymbol{y}\|_2^2+\frac{\lambda}{2}\|\boldsymbol{L}\boldsymbol{x}\|_2^2 \tag{3}$$

$$\boldsymbol{x}=(\boldsymbol{J}^T\boldsymbol{J}+\lambda\boldsymbol{L}^T\boldsymbol{L})^{-1}\boldsymbol{J}^T\boldsymbol{y} \tag{4}$$

In the preceding, the regularization term $\boldsymbol{R}$ has been replaced with the discrete approximation of the Laplace operator, $\boldsymbol{L}$. This minimization and regularization scheme is most commonly used in SHM literature [3] [6] [7] [8] [9] [10] [11] [12] [13] [14] [15] [16] [17] [18]. This particular formulation filters out highly oscillatory conductivity changes giving rise to smoothly varying images.

L2 ERROR NORM AND L1 REGULARIZATION NORM

Next, revisit equation (2) with $m=2$ and $n=1$ which corresponds to minimizing the error term in the least-squares sense while treating the l_1-norm of the regularization term. This approach often employs total variation regularization in order to permit discontinuous conductivity reconstructions. The primal-dual interior point method (PDIPM) [21] [22] [24] is typically used to find $\boldsymbol{x}$ in this approach by solving for the conductivity change as the primal problem while a secondary or dual optimization problem is simultaneously solved. Furthermore, the conductivity change, $\boldsymbol{x}$, is not solved for in one step. Rather, $\boldsymbol{x}$ is found by iteratively updating it by some small increment, $\delta\boldsymbol{x}$. Let the dual variable be denoted as $\boldsymbol{v}$. The primal minimization problem is shown in equation (5) and the corresponding dual problem is shown in equation (6).

$$\arg\min_{\boldsymbol{x}} \frac{1}{2}\|\boldsymbol{J}\boldsymbol{x}-\boldsymbol{y}\|_2^2+\lambda\|\boldsymbol{T}\boldsymbol{V}\boldsymbol{x}\|_1^1 \tag{5}$$

$$\arg\max_{\boldsymbol{v}} \begin{cases} \frac{1}{2}\|\boldsymbol{J}\boldsymbol{x}-\boldsymbol{y}\|_2^2+\lambda\boldsymbol{v}^T\boldsymbol{T}\boldsymbol{V}\boldsymbol{x}: \ |v_i|\leq 1 \\ \boldsymbol{J}^T(\boldsymbol{J}\boldsymbol{x}-\boldsymbol{y})+\lambda\boldsymbol{T}\boldsymbol{V}^T\boldsymbol{v}=0 \end{cases} \tag{6}$$

In equations (5) and (6), $\boldsymbol{TV}$ represents the discrete approximation of the total variation. In its continuous form, the total variation is $TV(x)=\int_\Omega|\nabla x|\,\mathrm{d}\Omega$ where Ω denotes the domain being imaged. A description of how to form its discrete version can be found in reference [21] by Borsic et al. Updates to both the primal and dual variables can be found in references [21] [22]. This approach is expected to be vulnerable to outlier data but capable of reconstructing discontinuous conductivity changes.

L1 ERROR NORM AND L2 REGULARIZATION NORM

Next, consider equation (2) with $m=1$ and $n=2$. This amounts to minimizing the l_1-norm of the error while treating the l_2-norm of the regularization. The discrete Laplace operator is again used for regularization. Similar the previous case for $m=2$ and $n=1$, a dual optimization problem is formed. The primal and dual problems can be respectively stated as follows where $\boldsymbol{z}$ is the new dual variable [22]. The primal

and dual variable updates can be solved for simultaneously as described in reference [22].

$$\arg\min_{\boldsymbol{x}} \|\boldsymbol{J}\boldsymbol{x}-\boldsymbol{y}\|_1^1 + \frac{\lambda}{2}\|\boldsymbol{L}\boldsymbol{x}\|_2^2 \tag{7}$$

$$\arg\max_{\boldsymbol{z}} \begin{cases} \boldsymbol{z}^T(\boldsymbol{J}\boldsymbol{x}-\boldsymbol{y}) + \frac{\lambda}{2}\|\boldsymbol{L}\boldsymbol{x}\|_2^2 \ : \ |z_i| \le 1 \\ \boldsymbol{J}^T\boldsymbol{z} + \lambda\boldsymbol{L}^T\boldsymbol{L}\boldsymbol{x} = 0 \end{cases} \tag{8}$$

Because of this particular combination of norms, this approach is expected to be robust to outlier data while promoting spatially smooth conductivity changes.

L1 ERROR NORM AND L1 REGULARIZATION NORM

Lastly, consider the case for $m = 1$ and $n = 1$. This corresponds to minimizing the l_1-norm of the error and the l_1-norm of the regularization. To solve this problem, one primal parameter, $\boldsymbol{x}$, and two dual parameters, $\boldsymbol{v}$ and $\boldsymbol{z}$, are constructed as follows [22]. The primal and dual iterative updates can be obtained from reference [22].

$$\arg\min_{\boldsymbol{x}} \|\boldsymbol{J}\boldsymbol{x}-\boldsymbol{y}\|_1^1 + \lambda\|\boldsymbol{T}\boldsymbol{V}\boldsymbol{x}\|_1^1 \tag{9}$$

$$\arg\max_{\boldsymbol{z},\ \boldsymbol{v}} \begin{cases} \boldsymbol{z}^T(\boldsymbol{J}\boldsymbol{x}-\boldsymbol{y}) + \lambda\boldsymbol{v}^T\boldsymbol{T}\boldsymbol{V}\boldsymbol{x} : \ |z_i| \le 1, |v_i| \le 1 \\ \boldsymbol{J}^T\boldsymbol{z} + \lambda\boldsymbol{T}\boldsymbol{V}^T\boldsymbol{v} = 0 \end{cases} \tag{10}$$

Due to the use of the l_1-norm for both the error minimization and regularization terms, this approach is expected to be robust to outlier data while also capable of imaging discontinuous conductivity changes.

APPLICATION TO CARBON BLACK-MODIFIED GLASS FIBER/EPOXY

To explore the effect of different error and regularization norms on damage identification in fiber-reinforced composites, the previously described EIT formulations are applied to a glass fiber/epoxy laminate that has been modified with CB nanofillers and subjected to a low-velocity impact [17]. This specimen was manufactured using unidirectional E-glass (225 g/m^2 areal weight), 0.5 wt.% high-structure CB filler, a stacking sequence of $[[0/90]_6/0]_s$, and measured 101 mm × 152 mm × 4 mm. The specimen was instrumented with a 16-electrode measurement system and impacted via drop-tower at 50 J. Further experimental details can be found in the original manuscript by Tallman et al. [17]. The post-impacted specimen is shown in Figure 1. Due to the impact, a visible indentation can be seen at the impact location. Crack damage is also visible on the surface of the plate.

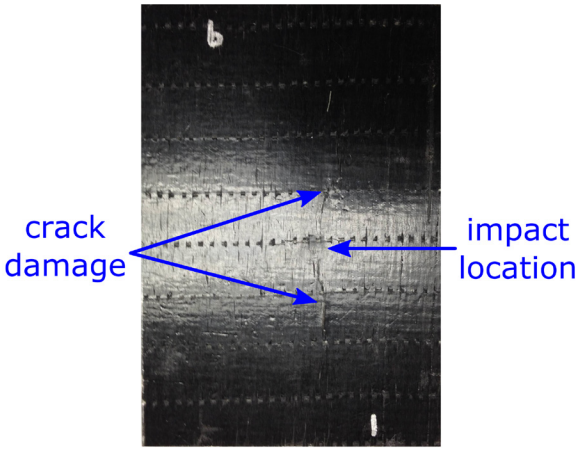

Figure 1. CB-modified glass fiber/epoxy laminate with visible indentation at the impact location and crack damage.

This damage state is visualized via EIT using all combinations of error minimization and regularization norms. The result of these different error and regularization norms can be seen in Figure 2. Furthermore, because the damage is expected to result in a conductivity loss, $\boldsymbol{x}$ is constrained to be non-negative for each combination of m and n.

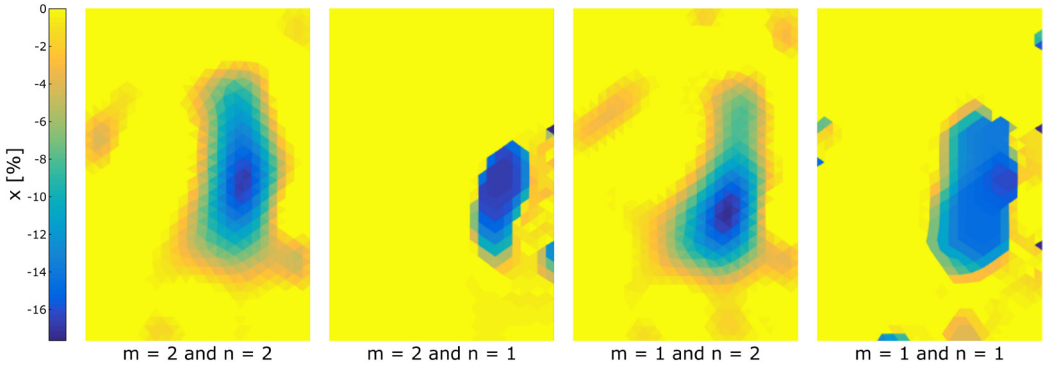

Figure 2. Impact damage induced conductivity losses in CB-modified glass fiber/epoxy laminate composite as imaged with EIT using all error minimization and regularization norms.

An interesting observation can be made from Figure 2. That is, although it might be expected that conductivity changes due to impact damage should be discontinuous (i.e. complete cessation of conductivity due to fractures), the images corresponding to $n = 1$ are qualitatively no better than the smoothly varying images corresponding to $n = 2$. This may be due to the fact that impact damage in a fiber-reinforced composite is a complicated collection of micro-cracks, fractures, and delaminations. These damages are seemingly more concentrated in the immediate vicinity of the impact but become less concentrated away from the impact location. As such, the net effect of the impact is likely smoothly varying from highly concentrated cracking near the impact location to much sparser cracking away from the impact location. Inasmuch, images using the l_2-norm on the regularization best capture this.

INCLUSION OF FAULTY ELECTRODE DATA

Lastly, the effect of faulty data due to damage electrodes is considered. Although care was taken in collecting the original data such that it is free of outliers, the consideration of outlier data is important in SHM applications because damaged electrodes may generate erroneous data. Here, the original experimental data is manipulated to include one strong outlier so that the effect of this on each error minimization and regularization norm combination can be investigated. Figure 3 shows the effect of a strong outlier measurement on the imaging of impact damage in the same glass-fiber/epoxy laminate.

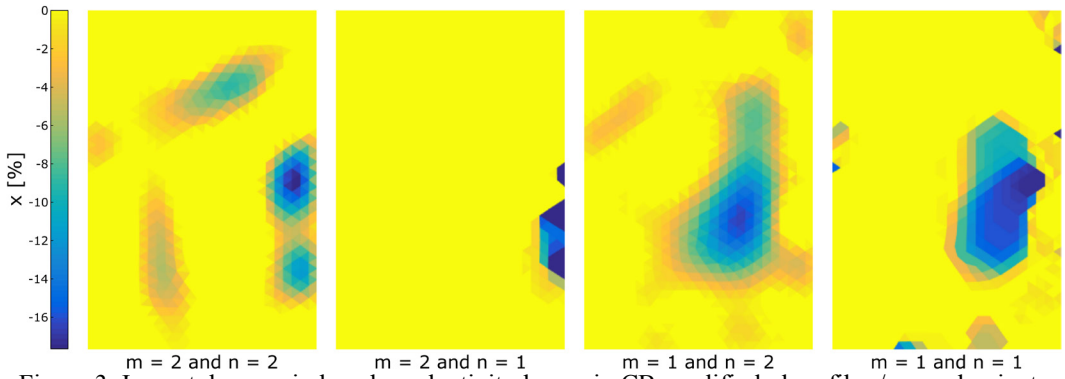

Figure 3. Impact damage induced conductivity losses in CB-modified glass fiber/epoxy laminate composite as imaged with EIT using all error minimization and regularization norms and with the inclusion of a strong outlier measurement due to a faulty or damaged electrode.

As can be seen from Figure 3, images using the l_2-norm of the error minimization do not produce any sort of physically meaningful image with the inclusion of an outlier measurement. On the other hand, the images using the l_1-norm for the error minimization are unaffected. This consistent with the expectations of each error norm and demonstrates the vulnerability of EIT formulations using l_2-norms for error minimization in SHM.

SUMMARY AND CONCLUSIONS

This manuscript has considered the effect of different error minimization and regularization norms for damage identification via EIT in glass fiber/epoxy laminates. To this end, four different combinations of error and regularization norms were used for visualizing impact-induced damage in a glass fiber/epoxy laminate modified with CB filler. All combinations of error and regularization norms accurately located the impact location. However, a qualitative assessment indicated that methods using the l_2-norm for regularization more satisfactorily captured the crack damage that resulted from the impact. At first glance, this may seem counter intuitive since the impact results in cracks, fractures, and delaminations all of which represent a discontinuous conductivity loss. However, it is speculated that while these damage events do indeed individually represent discontinuous conductivity losses, they are collectively acting as a complicated network of small damages. This network is very dense in the immediate vicinity of the impact and gradually becomes sparser

away from the impact location. Therefore, the net conductivity change is smoothly varying.

Lastly, the effect of a strong outlier measurement on image reconstruction was investigated because of the possibility of damaged electrodes in SHM applications. For this, EIT images were reformed with the inclusion of one strong outlier. This significantly affected the images using the l_2-norm for error minimization to the point that damage-induced conductivity changes were not discernable. Conversely, images produced using the l_1-norm for error minimization were not affected by the inclusion of a strong outlier.

Based on this investigation, it can be concluded that robust SHM systems should make use of the l_1-norm for error minimization in EIT. However, the norm of the regularization term may vary depending on the specific application. Therefore, a robust SHM system should have both l_1 and l_2-norms available to it.

REFERENCES

[1] F.-G. Yuan, Structural Health Monitoring (SHM) in Aerospace Structures, Elsevier, 2016.

[2] E. T. Thostenson and T.-W. Chou, "Carbon nanotube networks: sensing of distrbuted strain and damabe for life prediction and self healing," *Advanced Materials,* vol. 18, pp. 2837-2841, 2006.

[3] T. C. Hou and J. P. Lynch, "Electrical impedance tomographic methods for sensing strain fields and crack damage in cementitious structures," *Journal of Intelligent Material Systems and Structures,* vol. 20, pp. 1363-1379, 2009.

[4] M. Hallaji and M. Pour-Ghaz, "A new sensing skin for qualitative damage detection in concrete elements: rapid diference imaging with electrical resistance tomography," *NDT&E International,* vol. 68, pp. 13-21, 2014.

[5] M. Hallaji, A. Seppänen and M. Pour-Ghaz, "Electrical impedance tomography-based sensing skin for quantitative imaging of damage in concrete," *Smart Materials and Structures,* vol. 23, p. 085001, 2014.

[6] S. Gupta, J. G. Gonzalez and K. J. Loh, "Self-sensing concrete enabled by nano-engineered cement-aggregate interfaces," *Structural Health Monitoring,* 2016.

[7] M. Hallaji, A. Seppänen and M. Pour-Ghaz, "Electrical resistance tomography to monitor unsaturated moisture flow in cementitious materials," *Cement and Concrete Research,* vol. 69, pp. 10-18, 2015.

[8] T. C. Hou, K. J. Loh and J. P. Lynch, "Spatial conductivity mapping of carbon nanotube composite thin films by electrical impedance tomography for sensing applications," *Nanotechnology,* vol. 18, p. 315501, 2007.

[9] K. J. Loh, T. C. Hou, J. P. Lynch and N. A. Kotov, "Carbon nanotube sensing skins for spatial strain and impact damage identification," *Journal of Nondestructive Evaluation,* vol. 28, pp. 9-25, 2009.

[10] B. R. Loyola, T. M. Briggs, L. Arronche, K. J. Loh, V. La Saponara, G. O'Bryan and J. L. Skinner, "Detection of spatially distributed damage in fiber-reinforced polymer composites," *Structural Health Monitoring,* vol. 12, pp. 225-239, 2013.

[11] B. R. Loyola, V. La Saponara, K. J. Loh, T. M. Briggs, G. O'Bryan and J. L. Skinner, "Spatial sensing using electrical impedance tomography," *IEEE Sensors,* vol. 13, pp. 2357-2367, 2013.

[12] A. Baltopoulos, N. Polydorides, L. Pambaguian, A. Vavouliotis and V. Kostopoulos, "Damage identification in carbon fiber reinforced polymer plates using electrical resistance tomography mapping," *Journal of Composite Materials,* vol. 47, pp. 3285-3301, 2012.

[13] A. Baltopoulos, N. Polydorides, L. Pambaguian, A. Vavouliotis and V. Kostopoulos, "Exploiting carbon nanotube networks for damage assessment of fiber reinforced composites," *Composites Part B,* vol. 76, pp. 149-158, 2015.

[14] H. Dai, G. J. Gallo, T. Schumacher and E. T. Thostenson, "A novel methodology for spatial damage detection and imaging using a distributed carbon nanotube-based composite sensor combined with electrical impedance tomography," *Journal of Nondestructive Evaluation,* vol. 35, 2016.

[15] G. J. Gallo and E. T. Thostenson, "Spatial damage detection in electrically anisotropic fiber-reinforced composites using carbon nanotube networks," *Composite Structures,* 2015.

[16] T. N. Tallman, Gungor, W. K. W. S and C. E. Bakis, "Damage detection and conductivity evolution in carbon nanofiber epoxy via electrical impedance tomography," *Smart Materials and Structures,* vol. 23, p. 045034, 2014.

[17] T. N. Tallman, S. Gungor, K. W. Wang and C. E. Bakis, "Damage detection via electrical impedance tomography in glass fiber/epoxy laminates with carbon black filler," *Structural Health Monitoring,* vol. 14, pp. 100-109, 2014.

[18] T. N. Tallman, S. Gungor, K. W. Wang and C. E. Bakis, "Tactile imaging and distributed strain sensing in highly flexible carbon nanofiber/polyurethane nanocomposites," *Carbon,* vol. 95, pp. 485-493, 2015.

[19] T. N. Tallman and K. W. Wang, "Damage and strain identification in multifunctional materials via electrical impedance tomography with constrained sine wave solutions," *Structural Health Monitoring,* vol. 15, pp. 235-244, 2016.

[20] A. Adler and R. Guardo, "Electrical Impedance Tomography: Regularized Imaging and Contrast Detection," *IEEE Transactions on Medical Imaging,* vol. 15, pp. 170-179, 1996.

[21] A. Borsic, B. M. Graham, A. Adler and W. R. B. Lionheart, "In vivo Impedance Imaging with Total Variation Regularization," *IEEE Transactions on Medical Imaging,* pp. 44-54, 2010.

[22] Y. Mamatjan, A. Borsic, D. Gürsoy and A. Adler, "An experimental clinical evaluation of EIT imaging with l1 data and image norms," *Physiological Measurement,* pp. 1027-1039, 2013.

[23] D. S. Holder, Electrical Impedance Tomography: Methods, History and Applications, CRC Press, 2004.

[24] K. D. Andersen, E. Christiansen, A. R. Conn and M. L. Overton, "An efficient primal-dual interior-point method for minimizing a sum of Euclidean norms," *Journal on Scientific Computing,* pp. 243-262, 2000.